Charge constraints of macroscopic dark matter

Jagjit Singh Sidhu

Phys. Rev. D **101**, 043526 — Published 18 February 2020

DOI: 10.1103/PhysRevD.101.043526

Charge Constraints of Macroscopic Dark Matter

Jagjit Singh Sidhu
Physics Department/CERCA/ISO Case Western Reserve University Cleveland, Ohio 44106-7079, USA
(Dated: January 28, 2020)

Macroscopic dark matter (macros) refers to a broad class of alternative candidates to particle dark matter with still unprobed regions of parameter space. Prior work on macros has considered elastic scattering to be the dominant energy transfer mechanism in deriving constraints on the abundance of macros for some range of masses M_x and (geometric) cross-sections σ_x However, macros with a significant amount of electric charge would, through Coulomb interactions, interact strongly enough to have produced observable signals on terrestrial, galactic and cosmological scales. We determine the expected phenomenological signals and constrain the corresponding regions of parameter space, based on the lack of these signals in observations.

I. INTRODUCTION

The is strong evidence that dark matter is the dominant form of matter in the Universe (see e.g. [1]). Dark matter explains several phenomena on both galactic and cosmological scales [1], from the shape of galaxy rotation curves to the history of structure formation. However, the precise nature of dark matter remains one of the big unsolved problems in cosmology.

New fundamental particles, not included in the Standard Model of particle physics, are popular candidates because they often arise in models of Beyond the Standard Model physics that were invented for independent reasons (e.g. the axion [2–4]). However, it remains an open possibility that dark matter is comprised instead entirely of macroscopic bound states.

Such bound states would avoid strong constraints on the self-interactions of dark matter by virtue of their low number density instead of any intrinsic weakness in their non-gravitational couplings. One such open possibility is that dark matter is comprised of macroscopic bound states of quarks or hadrons, as first proposed by Witten [5] as products of a first-order QCD phase transition, and later Lynn, Nelson, and Tetradis [6] and Lynn [7] again, who argued in the context of SU(3) chiral perturbation theory that "a bound state of baryons with a well-defined surface may conceivably form in the presence of kaon condensation." This would place the dark matter squarely within the Standard Model. Others have suggested non-Standard Model versions of such objects and their formation, for example incorporating the axion [8]. Additionally, it has been noted in reference [9] that in a simple Higgs-portal complex scalar dark matter model, a non-topological soliton state exists for dark matter. This work also considered one possible mechanism to produce macroscopic dark matter soliton states from early-universe dynamics, i.e. a first-order phase transition of electroweak (EW) symmetry [9]

Due to their large mass and low number density, macro detectors must be extremely large, experience extremely long integration times or be proficient at accumulating dark matter due to e.g. gravitationally-enhanced Sommerfield enhancement as in white dwarfs and neutron stars, to overcome the macros' low flux compared to typical particle dark matter.

In recent years the author and collaborators have determined the regions of macro parameter space that cannot constitute all of the dark matter based on several null observations in various experiments [10–13]. We have also discussed further ways to probe more of the remaining parameter space [14, 15]. These works assumed the dominant interaction to be elastic scattering and the interaction cross-section, was taken to be the geometric cross-section of the macro, i.e. $\sigma_{elastic} = \sigma_x$. For more details on recent work involving macros as viable dark matter candidates, we refer the reader to the works cited above and references therein. However, we begin by first briefly reviewing the existing constraints on derived from previous work.

For macro masses $M_x \leq 55\,\mathrm{g}$ careful examination of specimens of old mica for tracks made by passing dark matter [16, 17] has ruled out such objects as the primary dark-matter candidate (see Figure 1). For even smaller masses $M_x \leq 55 \times 10^{-4}\,\mathrm{g}$, a similar constraint was obtained [18] using the MACRO detector [19] For $M_x \gtrapprox 10^{21}\,\mathrm{g}$, a variety of microlensing searches have constrained the abundance of macros [20–24] from a lack of magnification of sources by a passing macro along the line of sight of the observer. *The most recent lensing constraints from M31 have recently been corrected taking into account a more realistic model for the source stars in M31 [25].*

A large region of parameter space was constrained by considering thermonuclear runaways triggered by macros incident on white dwarfs [18]. Dark matter-photon elastic interactions were used together with Planck cosmic microwave background data to constrain macros of sufficiently high reduced cross-section σ_x/M_x [26]. Prior work had already constrained a similar range of parameter space by showing that the consequence of dark matter interactions with standard model particles is to dampen the primordial matter fluctuations and essentially erase all structures below a given scale (see e.g. [27]). The region of parameter space where macros would have produced a devastating injury similar to a gunshot wound on the carefully monitored population of the western world was also recently constrained [12].

Recently, together with collaborators, we suggested how ultra-high-energy cosmic ray detectors that exploit atmospheric fluoresence could potentially be modified to probe parts of macro parameter space [14], including macros of nuclear density. This analysis has led to constraints already being placed using networks of cameras that were originally built to study bolides, i.e. extremely bright meteorites with absolute magnitude [13]. We have also suggested how the approach applied to mica [16, 17] could be applied to a larger, widely available sample of appropriate rock [15], and used to search for larger-mass macros. We have also identified additional regions of parameter space constrained by the duration between back-to-back superbursts (thermonuclear runaway on the outer surface of a neutron star) [28].

It is unlikely that macro masses beyond $\sim 10^9$ g could be probed by any purpose-built terrestrial detector assuming even an observation time of a century and a target area the size of the Earth. Terrestrial probes (eg. ancient rocks [15–17]) could have been continuously exposed for up to $\sim 3 \times 10^9$ years, but we are unlikely to carefully examine the more than $1\,\mathrm{km}^2$ that would be needed to push beyond $M_x \sim 10^9$ g. It will therefore require innovative thinking about astrophysical probes (eg. [18]) to probe the remaining unprobed parameter space at the very highest masses.

There remains a wide range of masses M_x and cross-sections σ_x that are currently unconstrained by all previous work.

Macros over a wide range of densities remain possible candidates to explain the problem of the nature of dark matter. The constraints on macro parameter space from elastic scattering are presented in Figure 1. Some of these constraints will be relevant to the results of this paper, as we discuss below.

In this work, we introduce an additional mechanism for energy deposition through electromagnetic interactions of charged macros with charge $Q_x e$ where e is the unit charge, and Q_x is a number.

The velocity distribution of macros has in prior works been assumed to follow a Maxwellian distribution of the form

$$f_{MB}(\mathbf{v}_x) = \left(\frac{1}{2\pi\sigma^2}\right)^{\frac{3}{2}} e^{-\left(\frac{v_x^2}{2\sigma^2}\right)}, \qquad (1)$$

where $\sqrt{2}\sigma \approx 250$ km s^{-1}[29]. We will continue with this assumption in this work.

Numerous papers have been written considering a variety of charged dark matter candidates. The vast majority of the constraints have been derived for particle dark matter candidates. For a review of some of the constraints light mass particles, see e.g. [30, 31] and references therein. We summarize some of the results in the literature here regarding previous work on charged dark matter candidates.

A unit electric charge for a dark matter candidate, to contribute the majority of the observed dark matter, is excluded if its mass is not very large (these excluded masses are predominantly in the range of particles masses, but extend to masses $M_x \leq 10^{-13}$ g). However, as we shall show dark matter candidates with a unit charge and much larger masses, or even charges much higher than $\sim e$ at much larger masses are allowed to still contribute all of the observed dark matter.

Charged massive particles (CHAMPs) with integer charge values have been considered (see e.g. [31]) and a variety of terrestrial and astrophysical constraints derived. Such bounds apply only to particles with $M \lesssim 10^{-13}$ g.

Millicharged candidates, i.e. particles with $\epsilon \ll e$ where ϵ is a fractional charge value, are constrained by many observations. Accelerator searches (e.g. one carried out at SLAC [32] designed specifically to detect millicharged objects) assumed the millicharged particles to be produced entirely via electromagnetic interactions and produced no results over the range of sensitivity. Constraints have also been derived from supernova 1987A [33], considering the millicharged particle to be a dark-sector particle with a small electric charge.

Others have considered charged Planck-scale relics (CPRs) [34], which are expected to be of approximately the planck mass and possess a charge-to-mass ratio of e/M_{pl}. Reference [34] derived projections for the maximum abundances of CPRs based on null observations of a variety of terrestrial experiments.

Concrete charged macro formation models include macros formed from the mechanisms described for neutral macros, e.g. thos described in references [6, 7, 35], that then acquire a charged by absorbing nuclei during their lifetime. Such a possible mechanism for absorbing additional nuclei is described in reference [35]. Indeed, if a macro consists of a bound state of nuclei, it is plausible that a collision with a nucleus could result in the absorption of that nucleus, thus increasing the net charge of the macro.

However, in this manuscript we will undertake a phenomenological approach and consider a broad range of parameters M_x, Q_x and σ_x. We determine the regions of parameter space where charged macros with $M_x \geq 10^{-13}$ g. are currently allowed to be the sole component of dark matter. Thus, the results presented here in Figures 2a- 2f, where we rule out some region of the $Q_x - M_x$ plane, are the regions of the parameter space where the existence of such charged objects can contribute only a sub-component of the dark matter. We are concerned only with $M_x \lesssim 10^{23}$ g, above which a variety of microlensing results [20–24] have ruled out macros as being the dominant form of dark matter.

Galactic dynamics have been used to constrain dark matter self-interactions. Investigations into the allowed strength of dark matter self-interactions have been conducted (see e.g [36]). The observation of an offset between the gas and dark matter in a merging cluster, such as 1E 0657-56 (a.k.a. the bullet cluster), arising because of the ram pressure acting on the gas but not

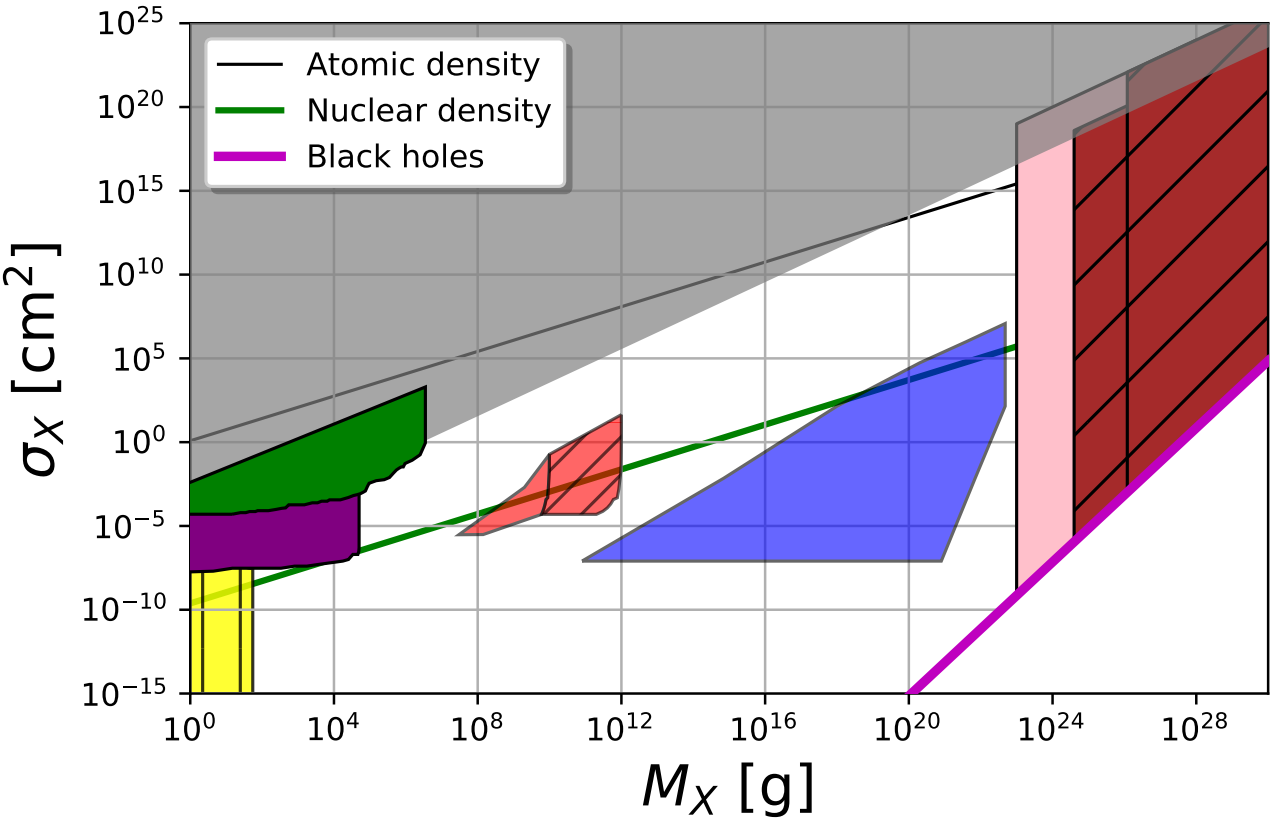

Figure 1: Constraints for macros considering elastic scattering to be the dominant interaction. Objects within the region in the bottom-right corner should not exist as they would simply be denser than black holes of the same mass. The various colored regions represent regions where macros cannot make up the entire amount of dark matter as their interactions through elastic scattering with their geometric cross-section σ_x would have produced observable consequences that have not been seen. The purple constraints are derived from a lack of human impacts [12], the green from a lack of fast-moving bolides events [13], the yellow from mica observation [16, 17], the red from superbursts [28], the dark blue from white dwarf supernovae [18], the grey from structure formation [26], the pink from microlensing of M31 [24, 25] and the maroon from microlensing [20–23]. See Section I for more details regarding these constraints.

the dark matter has been used to constrain dark matter self-interactions. Thus, macros with too high a charge content would be prohibited. We discuss the effect of electrically charged macros on galactic dynamics, resulting in an effect similar to the dynamical friction first discussed by Chandrashekar [37], and then by Binney and Tremaine [38]. We derive the analogous expressions for the drag force experienced by a charged macro travelling through a sea of other similarly charged macros, and relate this to an effective cross-section that we use to constrain the charged macros using the self-interaction constraints.

We show that charge bounds derived from the Cosmic Microwave Background (CMB) anisotropies that were determined for objects of much lower mass [39] also apply to much larger mass objects. Charged particles with sufficiently strong coupling to baryons would participate in the acoustic oscillations of baryon-photon plasma. This would affect the CMB radiation anisotropies in several ways. Using this idea together with recent Planck data, reference [39] severely constrained the charge content of dark matter.

Considerations on galaxy cluster scale magnetic fields affecting the charged dark matter distributions within a cluster has led to tight bounds being placed on millicharged dark matter [40]. Bounds were obtained by requiring that the motion caused by the randomly oriented magnetic fields should not smear out the dark matter distribution governed by the gravitational interactions and also by demanding that the Lorentz force should not exceed the gravitational force in a cluster. We show that these bounds extend to much more massive dark matter candidates.

We then set bounds on the allowed regions of the

charge-mass parameter space considering some of the null results quoted above in Figure 1. For both the mica and MACRO results, macros with a sufficiently large charge content would have left a detectable track in either detector. A phenomenological law for ions moving at speeds of $\beta \sim 10^{-3}$ has been determined in [41] and will be used in deriving constraints on the allowed charges of light mass macros for these two detectors.

Macros incident on a neutron star would be moving at moderately relativistic speeds, $\beta \sim 0.7$, and could potentially trigger thermonuclear runaway, resulting in a phenomena known as a superburst. For ions moving quicker than $\beta \sim 0.01$, the Bethe equation is an accurate description of the linear energy deposition. We constrain the charge content of macros that would have otherwise initiated a superburst in a shorter time than observed [28].

For all the other constraints quoted above in Figure 1, the macro would be moving at speeds appropriate to the usage of the phenomenological fit in reference [41]. However, the threshold linear energy deposition for a signal is much higher, requiring a large value of Q_x. At such large values the phenomenological fit in [41] is not valid (as will be explained in more detail in section III where the theory behind the framework for calculating the linear energy deposition is reviewed). For a general review of the effects of ions passing through matter or for more details on the two frameworks discussed here, we refer the reader to reference [41].

The constraints placed in this paper are from purely phenomenological observations, independent of considerations of the binding energy a macro of a certain density. One should consider only macros that satisfy

$$\frac{Q_x^2 e^2}{r_x} < E_b \frac{M_x}{m_b}, \tag{2}$$

where $r_x = \sqrt{\frac{\sigma_x}{\pi}}$, E_b is the macro binding energy per baryon and $m_b \sim 938$ MeV is the mass of a baryon. However, theoretical considerations have failed to yield a model-independent formation mechanism for macros. Hence, the binding energy of a macro cannot be predicted in a model-independent way and so we ignore this consideration.

Since it is unclear what binding energy macros would have, we use nuclear binding energy as a binding energy of potential interest when plotting (2) in our results figures (as an equality) with $E_b = 8\,\mathrm{MeV}$, i.e. the binding energy of iron peak elements. However this line is purely for illustrative purposes; for such large masses, the macro is much denser than nuclear density and so it is likely that the continued existence of such objects over cosmological timescales requires binding energies much higher than that corresponding to nuclear density objects.

We use Gaussian-cgs units throughout this analysis. For simplicity, we consider all macros to be of the same mass M_x and charge Q_x (as well as geometric cross-section σ_x).

The rest of this paper is organized as follows. In Section II, we discuss constraints from large-scale structure. In section III, constraints are obtained from terrestrial observations and the time duration between back-to-back superbursts on 4U 1820-30. In Section IV, the results are presented, along with a discussion of their range of applicability. In Section V, we conclude.

II. LARGE SCALE STRUCTURE

Constraints from Self-interacting Dark Matter (SIDM)

SIDM was initially proposed to solve inconsistencies between the cold dark matter (CDM) paradigm predictions and observations of structures on scales below a few Mpc, including the missing-satellite problem [42]. The centres of SIDM haloes are expected to have constant-density isothermal cores that arise as kinetic energy is transmitted from the hot outer halo inward. This results in a diminished central density of the dark matter halo, an idea first raised in reference [42]. Such a scenario can happen if the reduced cross-section of the dark matter candidate, σ/M (valid for any dark matter candidate), is large enough for there to be a relatively high probability of scattering over a time comparable to the age of the halo.

The result of strong self-interactions is an offset between the bullet sub-cluster mass peak and galactic centroid; the absence of this observation in the actual cluster provides a limit on σ/M. Comparisons were also made between simulations with SIDM and the observed density profiles and substructure counts of other observed clusters, low-surface brightness spiral and dwarf-spheroidal galaxies in [43]. In both cases, bounds on the strength of the self-interaction generally prohibit dark matter self-interactions with reduced cross-sections

$$\frac{\sigma_{total}}{M_x} \geq 1\,\frac{cm^2}{gr}\,, \tag{3}$$

where σ_{total} is the total cross-section for all interaction mechanisms, e.g. elastic scattering σ_x and the Coulomb force. We will consider both contributions in this manuscript where relevant although in vast regions of parameter space either one dominates. We use the reduced cross-section value to place constraints on the allowed charge values of macros that would have altered galactic dynamics through strong self-interaction.

Dynamical friction historically refers to the deceleration of a massive object moving through a population of other objects due to gravitational interactions. This effect has been discussed in [37, 38]. Here, we consider a similar effect that arises from a charged macro moving through a population of other charged macros. We show that for sufficiently high values of Q_x, the self-interaction between charged macros would be sufficiently strong and is thus constrained. Such strong self-interactions would

result in a situation where the high velocity macros located in the outer halo lose energy to the more slowly moving macros located near the center of the galaxy, resulting in the central density being diminished as the macros in the inner regions migrate outwards.

The analogous expression for the deceleration experienced by a macro passing through a population of macros, all with the same charge content, is obtained by redoing the analysis in Chapter 7 of [38]. The expression is equivalent to the original equation except for the replacement

$$G^2(M+m)m \to \frac{2Q_x^4 e^4}{M_x^2}\,, \tag{4}$$

yielding

$$\frac{d\mathbf{v}_M}{dt} = -32\pi^2 log(\Lambda^2+1)\frac{Q_x^4 e^4}{M_x^2}\frac{\int_0^{v_M} F(\mathbf{v}_m) v_m^2 dv_m}{v_M^3}\mathbf{v}_M\,, \tag{5}$$

where

$$\Lambda = \frac{v_x^2 M_x b_{max}}{2Q_x^2 e^2}\,, \tag{6}$$

$\mathbf{v}_M$ is the velocity of the macro under consideration and $F(\mathbf{v}_m)$ is the phase space number density defined in [38] and differs from the velocity distribution (1) by a factor of the number density $n_x = \rho_{DM}/M_x$ (for macros of a single mass)

$$F(\mathbf{v}_m) = n_x f(\mathbf{v}_m)\,. \tag{7}$$

For a Maxwellian velocity distribution (1), the integration in (5) can be carried out analytically, yielding

$$\frac{d\mathbf{v}_M}{dt} = -\frac{8\pi log(\Lambda) Q_x^4 e^4 n_x}{M_x^2 v_M^3}\left[Erf(X) - \frac{2X}{\sqrt{\pi}}e^{-X^2}\right]\mathbf{v}_M\,, \tag{8}$$

where $X = \frac{v_x}{v_{vir}}$ and $Erf(X)$ is the error function. Generally, the quantity in square brackets will be of order $\mathcal{O}(0.1-1)$ provided v_x is not too small, i.e. for the majority of macros in the distribution (1). We make this simplifying assumption in the following calculations, i.e. that the quantity in the bracket ~ 0.1.

A crucial concept in this calculation is that the effect described above results in the macros in the outer halo experiencing a negative force, which is essentially a drag force. Thus, we relate the drag force derived in (8) to the expression for drag first derived by Epstein [44] for objects where the physical size, r, is significantly smaller than the average separation

$$L = n_x^{-\frac{1}{3}}\,, \tag{9}$$

i.e. $L \gg$ r. The Epstein drag force is

$$F_{drag} = \frac{4}{3}\rho_{DM}\sigma_{eff}\overline{v_x} v_{x,M} = M_x\frac{dv_M}{dt}\,, \tag{10}$$

where σ_{eff} is the effective cross-section due to the Coulomb interactions between a macro and all other macros in the population, $\overline{v_x}$ is the mean speed of the population of macros and v_M is the speed of the macro under consideration. The effective cross-section may be thought of as the equivalent geometric cross-section for macros to interact, through scattering, similarly to the charged macros interactions and produce similar galactic-scale consequences. We take $\overline{v_x} = 250\,\mathrm{km\ s^{-1}}$. For the fast moving macros in the galactic population, assuming $v_M = 250\,\mathrm{km\ s^{-1}}$ will result in an underestimate of at most a factor of $\mathcal{O}(2-3)$. Thus, for simplicity, we take $v_M = 250\,\mathrm{km\ s^{-1}}$.

The effective reduced cross-section can be obtained by equating this drag force to the expression for Epstein drag (10) yielding

$$4\pi\frac{e^4}{v_M^4}\frac{Q_x^4}{M_x^3} = \frac{\sigma_{eff}}{M_x}\,. \tag{11}$$

By requiring the effective reduced cross-section to be greater than the threshold (3), we obtain

$$Q_x \geq 3\times 10^{16}\left(\frac{M_x}{gr}\right)^{\frac{3}{4}} \tag{12}$$

to not be ruled out by self-interaction constraints. This constraint is represented in purple in the results figures.

We have considered how sufficiently charged macros would cause deviations from the observed dark matter density profile. Thus, this constraint depends on how well the dark matter density profile can be measured. Currently, this quantity is known at best to to an accuracy of $10-50\%$ [45]. Thus, we can say with certainty that for the range of parameter space for which the constraints apply, charged macros make up at most a subcomponent of $\sim 10-50\%$ of dark matter.

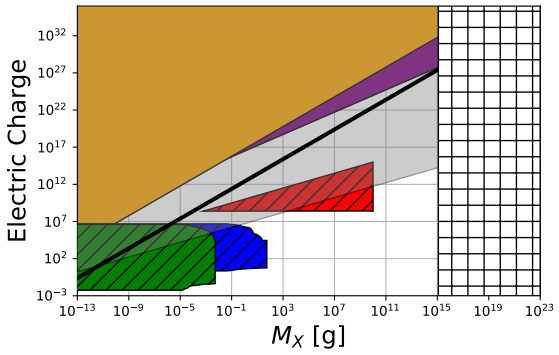

(a) $\sigma_x = 10^{-25}\,\mathrm{cm}^2$

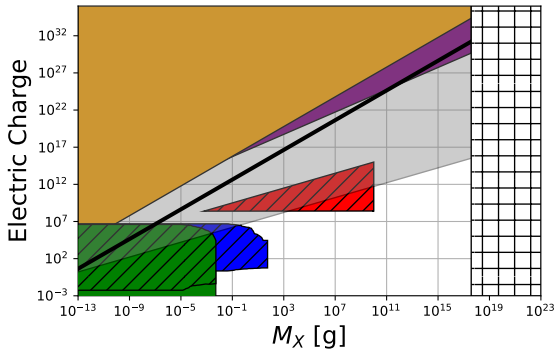

(b) $\sigma_x = 10^{-20}\,\mathrm{cm}^2$

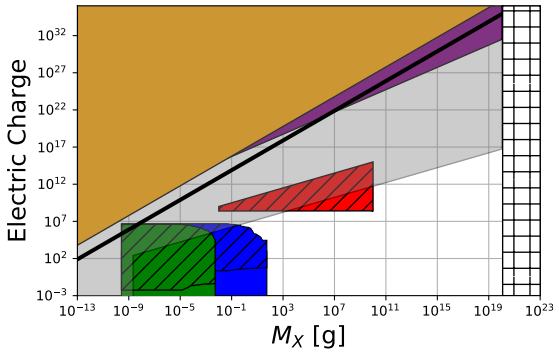

(c) $\sigma_x = 10^{-15}\,\mathrm{cm}^2$

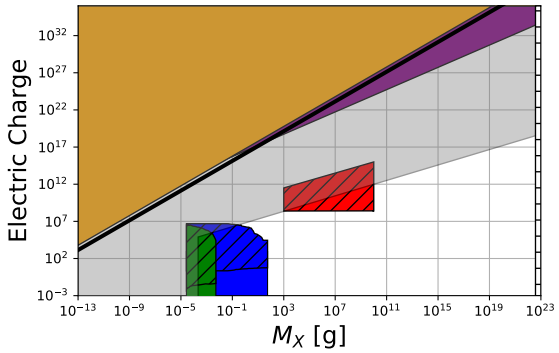

(d) $\sigma_x = 10^{-10}\,\mathrm{cm}^2$

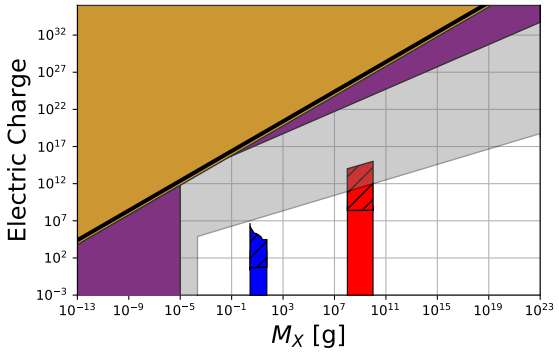

(e) $\sigma_x = 10^{-5}\,\mathrm{cm}^2$

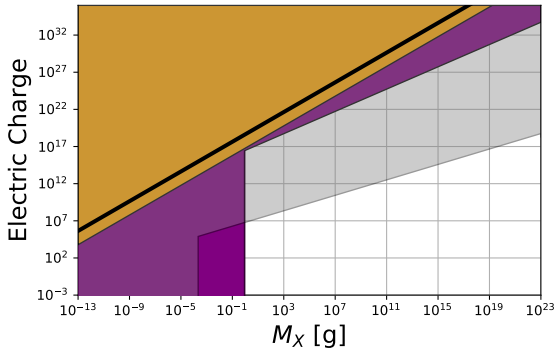

(f) $\sigma_x = 10^{0}\,\mathrm{cm}^2$

Figure 2: Constraints on the charge content of macros for several different values of the geometric (and elastic) cross-section σ_x. Constraints in yellow are derived from requiring charged dark matter not alter dynamics of galaxy clusters [40], in purple from requiring charged dark matter not interact too strongly with itself, in grey from CMB anisotropy considerations [39], in green from a null result of the MACRO detector, in blue from a null result of tracks in ancient muscovite mica and in red from the time between back-to-back superbursts on 4U 1820-30. The black line represents objects with binding energy $E_b = 8\,\mathrm{MeV}$, i.e. nuclear binding energy satisfying (2). Objects with masses greater than a critical threshold (44) should not exist as they would be denser than black holes of the same Schwarzchild radius. The hatching of the mica, MACRO and superbursts constraints refers to constraints derived in this work from electromagnetic interactions and not elastic scattering as in prior work on macros. Those are presented, where relevant, in the same respective color as the three aforementioned constraints but with no hatching.

CMB constraints

Reference [39] derived bounds on the charge of millicharged particles based on CMB anisotropy measurements and using data from Planck. However, charged dark matter objects, regardless of their mass, scatter off electrons and photons at the epoch of recombination. It was shown [39] that if the velocity transfer rate of this process exceeds the expansion rate of the Universe, the millicharged particles behave similarly to baryons until recombination.

This was used to constrain the charge content of millicharged particles. This bound may be restated as

$$Q_x \geq 5 \times 10^6 \left(\frac{M_x}{gr}\right)^{\frac{1}{2}} . \tag{13}$$

To justify the application of this bound to charged macros, which can be much larger than even Planck mass objects, the diffusion time, t_{diff}, for a photon to cross this average separation must be short compared to the relevant Hubble time. We assume that the Hubble time is that which corresponds to a radiation dominated Universe for simplicity

$$H^2 = H_0^2 (1+z)^4 , \tag{14}$$

where $H_0 \sim 70\,\mathrm{km\ s^{-1}\ Mpc^{-1}}$ [46] is the value of the Hubble constant today.

The average macro separation is determined from the number density of a distribution of macros of a single mass (9). The diffusion time for a photon, interacting with a mean free path

$$\lambda_{MFP} = (n_e \sigma_T)^{-1} , \tag{15}$$

where n_e is the electron number density and σ_T is the Thomson scattering cross-section, is

$$\tau_{diff} = \frac{L_{DM}^2}{\lambda_{MFP} c} , \tag{16}$$

where the quantity in the denominator is the thermal diffusivity.

Requiring (16) to be small compared to the Hubble time, H^{-1} yields

$$n_e \sigma_T n_x^{-\frac{2}{3}} c^{-1} H \ll 1 \tag{17}$$

In terms of the Macro mass this inequality may be written as approximately

$$\left(\frac{M_x}{gr}\right)^{\frac{2}{3}} (1+z)^3 \ll 10^{39}. \tag{18}$$

For the large Macro candidates of $M_x \sim 10^{25}\,\mathrm{g}$, i.e. much greater than masses we are interested in probing, $t_{diff,DM} \leq H^{-1}$ remains true for $\mathrm{z} \geq 10^7$. Thus, the large dark matter masses considered here do not ruin the dark matter fluid approximation and the constraints originally derived for particle mass dark matter applies equally to macros at redshift $z \sim 1100$ when recombination took place.

However, the constraints from the CMB differ from all other constraints in this manuscript in one way: the CMB constraints are from the early Universe while all other constraints are from the late Universe. We would require some formation mechanism capable of producing charged macros in the required abundance by the era of recombination to consider the CMB constraints on the same footing as the other constraints. Thus, we present the CMB constraints in the results figures in light shading to show that the CMB constraints are subject to additional scrutiny.

The original constraints limited the abundance of millicharged dark matter to 0.2% over the range of applicability of the constraint. This result thus also applies to charged macros.

Large Scale Magnetic Fields

A stringent bound was placed on the charge content of dark matter in [40] using magnetic fields in galaxy clusters. Since magnetic fields of $B \sim 1\,\mu G$ typically exist in clusters, upper bounds on the charge of dark matter were derived by looking into the effects of the magnetic on the charged dark matter.

In particular, the constraints were derived by requiring that the motion induced by the magnetic fields should not change the charged dark matter distribution governed by the gravitational interactions. Similar constraints were derived by requiring the Lorentz force not exceed the gravitational force in a cluster, since dark matter interacts predominantly through gravity on such scales. Charged dark matter with

$$Q_x \geq 10^{16} \left(\frac{M_x}{g}\right) \tag{19}$$

were ruled out based on this analysis.

To justify the application of this bound to macros over the mass range of interest, which is much larger than the masses considered in reference [40], we must justify the dark matter fluid approximation. We must demonstrate that the physical volumes considered are larger than n_x^{-1} since we are using the distribution of the dark matter to place constraints. Given an average cosmological dark matter density of $2 \times 10^{-30}\ \mathrm{g\ cm^3}$ and a maximum macro mass of interest $10^{21}\,\mathrm{g}$, we must consider comoving volumes greater than of order 1 pc which is true of the probe considered here.

This bound is stronger than the bound from self-interactions for $M_x \lesssim 1\,\mathrm{gr}$.

Similar to the constraint derived from self-interactions, this constraint also depends on how well the dark matter density profile is known and so the same maximum abun-

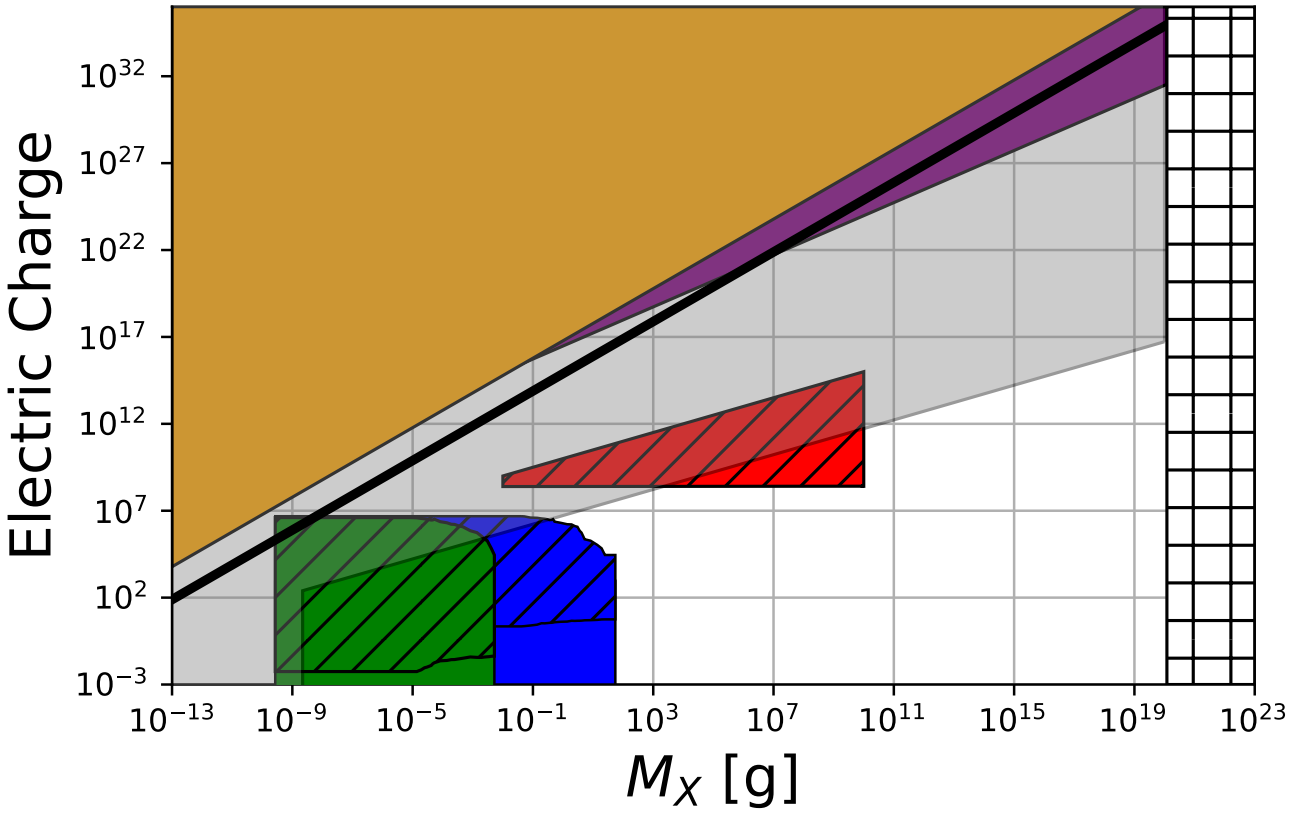

Figure 3: Constraints on the charge content of macros for geometric (and elastic) cross-section $\sigma_x = 10^{-15}\,\mathrm{cm}^2$. Constraints in yellow are derived from requiring charged dark matter not alter dynamics of galaxy clusters [40], in purple from requiring charged dark matter not interact too strongly with itself, in grey from CMB anisotropy considerations [39], in green from a null result of the MACRO detector, in blue from a null result of tracks in ancient muscovite mica and in red from the time between back-to-back superbursts on 4U 1820-30. The black line represents objects with binding energy $E_b = 8\,\mathrm{MeV}$, i.e. nuclear binding energy satisfying (2). Objects with masses greater than $M_x \sim 1.2 \times 10^{20}\,\mathrm{g}$ should not exist as they would be denser than black holes of the same Schwarzchild radius.

dance of charged macros as dark matter can be inferred for this constraint.

III. ENERGY DEPOSITION ALONG TRACKS OF CHARGED OBJECTS

In this section, we are concerned with localized terrestrial and astrophysical detectors where the linear energy deposition of a passing macro would exceed some critical threshold and leave an observable signal. The linear energy deposition is now the sum of the two separate contributions

$$\frac{dE}{dx} = \left.\frac{dE}{dx}\right|_{elastic} + \left.\frac{dE}{dx}\right|_{Coulomb}. \tag{20}$$

We are most interested in cases where the second term alone exceeds the threshold energy deposition for a track to be produced in our detector. However, we will also consider cases where the first term dominates, i.e. cases where a large but neutral macro would have triggered the detector through elastic scattering.

As discussed in [1, 41], the speed of a passing ion determines the amount of energy transferred on passing through a material. This is primarily because different energy transfer mechanisms dominate at different speeds (see additionally e.g. [47, 48] for a discussion of the differences between electronic and nuclear stopping). We first discuss macros moving slowly $\beta \sim 10^{-3}$ before proceeding to the moderately relativistic version $\beta \sim 0.7$. The form of the second linear energy deposition term in (20) will be different for each of these cases.

Non-relativistic macros

Reference [41] has produced a reasonably accurate model of the energy transfer of low energy ions by taking

into account the complex electronic screening potential. The goal of reference [41] was to produce a single analytic function for the interatomic potential, thus allowing a single formula for the nuclear stopping to be determined, as opposed to using a separate function for each ion-atom pair.

The potential of the two particles can also be reduced to that of a single potential called the Interatomic Potential [41]. Each of these potentials may be considered as a Coulombic term multiplied by a screening function, due to electronic screening that reduces the effects of the nuclear Coulombic term at all radii. The screening function is related to the interatomic potential through

$$\Phi = \frac{V(r)}{Z_1 Z_2 e^2/r}\,, \tag{21}$$

where Z_1 and Z_2 are the bare charge of the two interacting nuclei (in our case we take $Z_1 = Q_x$) and r is the distance between the nuclei. The interatomic function is generally found by using simple atomic potentials and adjusting the definition of the screening length to approximate the two-atom potential.

To obtain one analytic function to describe nuclear stopping in all ion-atom pairs, a large sample of ion-atoms pairs were chosen and the detailed potential calculated using computer simulations [41]. Various screened potentials of the form

$$\Phi(x) = f(x)\,, \tag{22}$$

where $x = \frac{r}{a_{screen}}$ and a_{screen} is a screening length, which is a parameter that characterizes the radial spread of the electronic charge about the radius [41], were then trialed to determine the screening potential that most closely matched all the pairs. The screening function that was determined to best fit the pairs

$$\Phi(x) = 0.1818e^{-3.2x} + 0.5099e^{-0.9423x} + 0.2802e^{-0.4028x} + 0.02817e^{-0.2016x} \tag{23}$$

had a screening length that was determined to be

$$a_u = 0.8853 a_0 \frac{1}{Q_x^{0.23} + Z_2^{0.23}}\,, \tag{24}$$

where a_0 is the Bohr radius. This quantity was determined to be the one with the appropriate Z dependence to best reproduce the results of the numerically calculated potentials from the 522 atomic pairs. The screened potential was determined to deviate from experimental measurements by at most 18% [41], which is sufficient for the purpose of this manuscript.

With the universal screening potential, the energy transferred due to the two scattering of the two particles can be calculated as

$$S_n(E) = \int_0^\infty T d\sigma\,, \tag{25}$$

where T is the energy transfer by the passing macro and $d\sigma = 2\pi b\, db$. The stopping power in (25) is related to the linear energy deposition through

$$\left.\frac{dE}{dx}\right|_{Coulomb} = N S_n(E)\,, \tag{26}$$

where N is the number density of atoms.

Results are generally presented in terms of a reduced energy, ϵ, and a corresponding stopping power $S(\epsilon)$. These are related to the physical versions of these quantities through

$$\epsilon = \frac{a_u E_0 M_2}{Q_x Z_2 e^2 (M_x + M_2)}\,, \tag{27}$$

and

$$S(\epsilon) = \frac{\epsilon}{\pi a_u^2 \gamma E_0} S(E_0)\,, \tag{28}$$

where a_u is the universal screening length in (24). The purpose for converting to a reduced coordinate system was to better show the results of using classical charge distributions and solid state distributions, which was also done for the first time in the calculations of [41]. In such a coordinate system, a single curve describes all combination of atom-atom collisions.

For ease of calculation, an analytic fit to the solution of the reduced stopping power was given

$$S_n(\epsilon) = log\frac{(1 + a\epsilon)}{\epsilon + b\epsilon^c + d\epsilon^e}\,, \tag{29}$$

where the best-fit coefficients were determined to be $a = 1.1383$, $b = 0.01321$, $c = 0.21226$, $d = 0.19593$ and $e = 0.5$.

This function is related back to the physical stopping power through

$$S_n(E_0) = \frac{8.462 \times 10^{-15} Z_1 Z_2 M_2 S_n(\epsilon)}{M_1 + M_2 (Z_1^{0.23} + Z_2^{0.23}} \frac{eV}{\frac{atom}{cm^2}}. \tag{30}$$

It is this function that we have used in determining the minimum value of Q_x for a macro to have a left a detectable track in the MACRO experiment and slab of mica, together with an approximate value of $N \sim 10^{23}$ atoms cm^{-3} in both cases.

This fitting procedure is valid only for $\epsilon \gtrapprox 10^{-5}$, below which larger charges produce smaller energy depositions. This can be seen by taking the low ϵ limit of (29), the

middle term in the denominator dominates for $\epsilon \gtrapprox 10^{-5}$. Thus, (29) becomes

$$S_n(\epsilon) \propto \epsilon^{0.78774}\,, \tag{31}$$

which results in

$$S_n(E) \propto Q_x^{-0.01774}\,. \tag{32}$$

Thus, larger values of Q_x reduce the energy transfered to the surrounding medium and we truncate our analysis once the value of $\epsilon \sim 10^{-5}$ because one would expect that larger values of Q_x would deposit more energy in the surrounding medium. The phenomenological law breaks down in this regime of $\epsilon \leq 10^{-5}$.

The procedure described in [41] was performed using 522 pairs of atom. Experimental verification has been conducted using various ion-atom pairs. However, the results derived here will be at charge values far above those tested and verified. It is thus quite possible that we are extending the results of [41] into a region of parameter space where it is not an accurate description of interactions between ions and atoms. Nonetheless, it is reasonable to suggest that at such large charge values, energy deposition would indeed be high. Thus, although the tools used may not be accurate, these tools are currently the best tools available and we utilize them to the full extent permitted.

The preceding discussion is relevant to both the MACRO detector, and ancient muscovite mica, which we discuss next.

MACRO and mica

Macros of a sufficiently low mass would have left an observable signature on Earth. If they have a low enough σ_x/M_x and charge value Q_x so that they would have penetrated deep (a few km) into the Earth's crust, a record would have been left in the MACRO experiment and ancient muscovite mica. We will use the lack of a track in both these detectors to constrain the charge content of macros of low masses.

MACRO was a large multipurpose underground detector located in the Hall B of the Laboratori Nazionali del Gran Sasso (Italy); it was optimized for the search of GUT magnetic monopoles with velocity $\beta \geq 4 \times 10^5$ [19]. A track that would have been detectable by etching measurements would have been left by macros that deposited a minimum nuclear component of stopping power

$$\frac{dE}{dx} \sim 5 \frac{\text{MeV}}{\text{cm}}\,. \tag{33}$$

However, the MACRO experiment obtained a null result and due to the extreme sensitivity of the detector, constraints were placed on extremely small macros from elastic scattering in [18].

Similarly, ancient muscovite mica was used to constrain macro parameter space [10] based on the null result of tracks when an etching technique was applied to look originally for lattice defects produced by passing magnetic monopoles predicted by Grand Unified Theories [16, 17]. A track would have been left by macros with a linear energy deposition [10]

$$\frac{dE}{dx} \sim 10 \frac{\text{GeV}}{\text{cm}}\,. \tag{34}$$

These thresholds of linear energy deposition will be used in this manuscript to constrain the charge values of macros that would have left a track independent of the geometric cross-section σ_x.

Lack of constraints for other non-relativistic macro scenarios

In Figure 1, there exist constraints on the abundance of macros from numerous other observations including the continued existence of white dwarfs, the lack of fast-moving bolides in meteorite surveys and a lack of unexplained human deaths.

However, in all cases other than that of MACRO and mica, we are unable to derive a minimum possible value of Q_x. Hence, we are also unable to determine the maximum Q_x for a charged macro to not lose most of its momentum and stop before reaching the appropriate depth.

We are unable to determine a lower bound on Q_x because the amount of charge for a macro to be capable of producing any of the aforementioned events is too large as a much higher threshold linear energy deposition is required than either (33) or (34). For such large Q_x values, the phenomenological law breaks down as it enters a region where it's validity is questioned. Such large values of Q_x result in $\epsilon \lesssim 10^{-5}$, where the theory results in predictions that are counter-intuitive (see discussion around equations (31)and (32)). Thus although it seems likely that some range of charges might be constrained by these observations, there is currently no theory capable of rigorously predicting this range. Thus, we do not use any of the other constraints from σ_x to place any constraints on the macro charge Q_x.

Moderately Relativistic macros

For moderately relativistic charged heavy particles, the energy loss is well described by the Bethe equation [1]. Classically, the derivation by Bohr assumed the electrons were stationary. The quantum mechanical version was later derived by Bethe and does not deviate significantly from the classical version where we are concerned. For the purpose of this section, we are concerned with the injection of a large amount of energy into ions near the surface of a neutron star with the purpose of triggering thermonuclear runaway resulting in a superburst. Thus, electronic corrections as in the shell-corrections, are not required. The density effect correction is also unimpor-

tant at such low (but still moderately relativistic) speeds [1].

Although one expects for moderately relativistic macros that the electronic energy transfer is stronger than the nuclear component, as mentioned above, we are interested in the carbon ions near the surface of a neutron star that can undergo thermonuclear runaway.

Considering a macro through the outer layer of a neutron star, the net momentum transfer experienced by the ions perpendicular to the direction of motion of the passing macro due to the Coulomb force,

$$E_{per} = \frac{Q_x e b}{(b^2 + (vt)^2)^{\frac{3}{2}}}\,, \tag{35}$$

is given as

$$p = \int_{-\infty}^{\infty} dt F_{per} = 2\frac{Z_1 Q_x e^2}{bv}\,. \tag{36}$$

In the non-relativistic limit where the energy transferred can be well approximated as just the classical component, the energy transferred is

$$\Delta E = \frac{p^2}{2m} = 2\frac{Z_1^2 Z_2^2 e^4}{b^2 v_x^2 m_c}\,. \tag{37}$$

To obtain the stopping power, $S_n(E)$, this energy transferred must be integrated over all impact parameters

$$S_n(E) = 2\pi \int \Delta E(b) b db \tag{38}$$

resulting in a linear energy deposition

$$\frac{dE}{dx} = \frac{4\pi N Z_1^2 Q_x^2 e^4}{m_C v_x^2} log\left(\frac{b_{max}}{b_{min}}\right)\,, \tag{39}$$

where N is the number density of atoms in the medium of the detector, Q_x is the charge of the macro, $m_C = 10^{-23}$ g is the mass of a carbon nucleus and b_{max} and b_{min} are the upper and lower limits of integration.

This is the classical form of the Bethe equation first derived by Bohr [41] and is sufficient for our purposes due to the simplifications mentioned previously.

To determine the limits of integration, we first summarize the theory behind thermonuclear runaway. As discussed in [18, 49], for thermonuclear runaway to be ignited, there is a minimum sized region (λ_{trig}) that must be raised above a threshold temperature $T_{crit} \sim 5\times10^9$ K for thermonuclear runaway to be initiated. (λ_{trig}) is strongly dependent on density. Thus, the upper limit is the trigger size. The lower limit in the logarithm is taken to be the physical size of the macro nuclei, i.e. the nuclei that are impacted head on by the macro (since by definition we are considering macros who elastic scattering cross-section is below the minimum size necessary to trigger thermonuclear runaway) are not important for the purposes of this manuscript. All nuclei around these central ones are of interest.

However, since the limits are only present in (39) inside the logarithm, the results derived here will be relatively insensitive to those limits. For the range of trigger sizes determined in [49, 50], the logarithm gives a factor $\sim$ 10, and we will use this approximation to simplify the analysis.

4U 1820-30

We use the time between back-to-back superbursts on a neutron star 4U 1820-30 to determine constraints on the charge content of dark matter of higher masses than previously constrained with terrestrial detectors.

A macro passing through 4U 1820-30 would have set off a superburst provided a linear energy deposition of

$$\frac{dE}{dx} \gtrapprox 6\times10^{22}\frac{MeV}{cm}\,, \tag{40}$$

had been deposited. This would have resulted in $\sim 10^8$ J of energy being deposited over a range of 10^{-4} cm, which was the trigger size for a density of $\rho \sim 10^8$ g cm^{-3} (insert citation here). For less dense regions in a neutron star crust, the energy requirement is higher but the general process for determining the threshold linear energy deposition is the same.

Accreting neutron stars undergo superbursts naturally once enough material has been accreted [28]. However, a macro incident on such a neutron star could trigger a superburst, which would not be as powerful as one caused by no external trigger. This idea was used to constrain intermediate mass macros based on the decade long duration between back-to-back superbursts on 4U 1820-30. However, there is one caveat to this [28] constraint as it is still unclear how superbursts are initiated. This is similar to the case of white dwarfs undergoing a type 1A supernova. It is unclear if the initiation of a deflagration wavefront is sufficient to trigger thermonuclear runaway in the entire carbon ocean. This will require further numerical work to determine if the region constrained is truly ruled out.

The constraints derived in this section all depend primarily on the flux of charged macros, i.e. they are proportional to M_x^{-1}. Thus the abundance of charged macros can be constrained as M_x^{-1}. This implies that the lower the charged macro mass constrained by these methods, the stronger is the limit on the maximum abundance of these objects as dark matter. Thus, smaller mass charged macros can contribute only as tiny subcomponents of dark matter.

IV. RESULTS

We first summarize the main parameter(s) that determine the constraints derived in this manuscript before discussing other aspects of these constraints.

The strongest constraint for millicharged dark matter (and hence charged macros) is the CMB constraints, which is an early Universe constraint and requires the dark matter to have been formed by this point (if not much earlier). The other two large scale structure constraints are both late Universe constraints. In general, millicharged dark matter constraints depends on both the charge Q_x and M_x. This is a reflection of the fact that these constraints depend on the charged macros in the distribution creating large scale effects. This means that what matters is the amount of "charge per unit mass". This is not an exact statement because the constraints depend on the charge per unit mass raised to various powers. However, this statement is schematically true.

The constraints from ancient mica, MACRO monopole searches and superbursts are dependent primarily on the flux of incident charged macros, i.e. the mass. Additionally, using the phenomenological law derived in reference [41] that was used to constrain charged macros utilizing null results from ancient mica and the MACRO monopole detector, the speed of the charged macros in the distribution determines the upper and lower bounds of the charge values that are constrained.

Applicability

Before we discuss the results, we first discuss the range of applicability of the results.

We first consider macros incident on either MACRO or mica as well as the outer layers of a neutron star. Considering elastic scattering alone, macros of a sufficiently large cross-section will be slowed before reaching the detector. This can be understood by considering the evolution of the velocity of a macro as it passes through a medium

$$v(x) = v_0 e^{-\langle \rho \Delta \rangle \frac{\sigma_x}{M_x}} \,, \tag{41}$$

where $\langle \rho \Delta \rangle$ is the integrated column density traversed defined as

$$\langle \rho \Delta \rangle = \int_l \rho(l) dx \,, \tag{42}$$

where l represents the trajectory of the macro, v_0 is the initial velocity of the macro and $\frac{\sigma_x}{M_x}$ is the reduced cross-section. Indeed, this is how the upper bounds are generally derived for the various exclusion regions in Figure 1.

A similar scenario is expected to manifest for macros with a significant amount of charge. If macros were to possess a large charge, they would have transferred a significant fraction of their initial energy to the overlying layers of rock or the outer layer of a neutron star and thus be slowed down before reaching the detector.

Thus, we will require,

$$\delta E \ll \frac{1}{2} M_x v_x^2 \,, \tag{43}$$

where the energy loss is from both mechanisms in (20). This criteria will be used in determining the upper bound on the charge constraints of a macro. These considerations for ancient mica and the MACRO experiment reveal that any upper bounds are similar to those derived by requiring that $\epsilon \lesssim 10^{-5}$.

For objects of a fixed physical size (and hence geometric cross-section), there is a maximum mass before the object becomes a black hole. This is illustrated in the results figures as the white hatched region on the right. The high mass boundary was determined by solving for the mass corresponding to the Schwarzchild radius[51]

$$M_{upper} = \sqrt{\frac{\sigma_x}{\pi}} \frac{c^2}{2G} \,. \tag{44}$$

Objects heavier than this mass should not exist, as they would be denser than black holes of the same Schwarzchild radius. These regions are hatched with + symbols in the results figures.

Presentation of results

In this work, we have introduced a third parameter to describe a physical attribute of a macro, Q_x. Thus, the results should be presented in a three dimensional parameter space. However, this will not be as informative as in the two dimensional analog when we considered only σ_x and M_x. Instead we present, as our results, the two dimensional parameter space of Q_x and M_x for slices of constant σ_x. We hope that by presenting results for several value of σ_x, that the overall picture of the constraints and their evolution as we change σ_x becomes clear to the reader.

For a given σ_x, there exists constraints for some range of M_x independent of the charge Q_x of the macro. Thus, some values of Q_x are constrained in abundance already by the elastic scattering considerations. This results in regions constrained for some range of masses upto some value of Q_x in Figures 2a - 2f, corresponding to the minimum Q_x values required for a track to have been left purely by Coulomb interactions. These constraints from elastic scattering are presented in the same color as the constraints from the charge of the macro but without the diagonal hatching. We note that Figure 2a is at a sufficiently low elastic cross-section σ_x that it is a characteristic result for all smaller elastic cross sections, i.e. these constraints apply to objects that are phenomenologically similar to the charged Planck-scale relics considered in reference [25]. If such objects existed and were not electrically charged, they would be particles with effectively no non-gravitational interaction with the constituents of the standard model.

The lower bounds in M_x come from the requirement that the macro not loose a significant fraction of its energy before reaching the appropriate depth in either the Earth (as in the case of the ancient mica or the MACRO detector) or a neutron star. Thus, for the constraints

from large scale structure, there is no lower bound on M_x for bounds from $\sigma_{elastic}$ independent of Coulomb interactions.

For the constraints derived using MACRO, mica and 4U 1820-30, a sufficiently large σ_x results in a minimum mass on the constraints due to the upper bound from (43) with the energy loss in this case dominated by elastic scattering.

We find that charges up to $Q_x \sim 10^6$ are constrained using the MACRO and mica null results. This is significantly above any values of Z that exist in the periodic table. However, it is reasonable to expect that larger values of Q_x would deposit more energy. Thus, one might expect that larger values of Q_x than those constrained here would also be ruled out based on the null observation of tracks in MACRO and mica. However, as our phenomenological model breaks down around $Q_x \sim 10^6$, we stop placing constraints at these Q_x values, even though it is likely constraints exist at larger values of Q_x. More conservatively, we expect the results to hold upto an atomic number of order $\mathcal{O}(100-1000)$; however, we present the entire range of constraints.

The neutron star constraints are at higher values of Q_x, mainly due to the higher linear energy deposition threshold value required to trigger thermonuclear runaway.

The results from large scale structure prohibit large values of Q_x/M_x. We plot both the results from self-interaction and ISM analysis because the CMB bound is subject to additional scrutiny. A theory describing the formation of macros in the early Universe is required for this bound to be taken at the same level of rigor as the other late Universe constraints.

We note that we are constraining objects with physical sizes below that which are normally associated with macroscopic dark matter [10], i.e. objects smaller than about the size of a nuclei.

Finally, we also note that our results constrain all charge values between the maximum and minimum limits and not only charge values $Q_x = ne$ or $Q_x = \frac{n}{3}e$, where n is an integer.

V. CONCLUSION

We have produced constraints on the maximum charge of macros from phenomenological considerations on a variety of scales. We have used galactic dynamics, CMB measurements and galaxy cluster considerations to constrain dark matter charge constraints on large scales. On terrestrial scales, the lack of any tracks observed in an slab of mica exposed to the bombardment exposed over geologic timescales, and in the MACRO experiment were also used to constrain small mass macros. Finally, the duration between back-to-back superbursts on 4U 1820-30 was used to constrain intermediate mass macros.

In Figures 2a-2f, we have shown the regions of parameter space where charged macro candidates cannot contribute all the dark matter that is observed on a variety of cosmological scales.

It is of particular interest to note that the results from MACRO seem to exclude macros over the appropriate mass range and geometric cross-sections from being charged at all, as these results exclude charges down to approximately $\frac{e}{3}$, which is the smallest known quantized charged value, assuming macros to me made of standard model particles.

It is interesting to return to the question of binding energies of macros first raised in Section I. Considering the results derived, and the line representing objects with iron peak elements binding energy in the result figures, we find that one would not expect objects with large Q_x values and small masses to be bound. However, the primary concern in this work has been to constrain the allowed charge values for macros to contribute all of the dark matter, based on purely observational grounds as there currently exists no concrete theory describing the formation of a macro and its subsequent binding energy.

VI. ACKNOWLEDGMENTS

This work was partially supported by Department of Energy grant de-sc0009946 to the particle astrophysics theory group at CWRU. The author would like to thank Alexis Plascencia, Pavel Fileviez Perez and Glenn Starkman for initial discussions on this manuscript.

[1] M. Tanabashi *et al.* (Particle Data Group), Phys. Rev. D **98**, 030001 (2018).
[2] R. D. Peccei and H. R. Quinn, Phys. Rev. Lett. **38**, 1440 (1977).
[3] F. Wilczek, Phys. Rev. Lett. **40**, 279 (1978).
[4] S. Weinberg, Phys. Rev. Lett. **40**, 223 (1978).
[5] E. Witten, Physical Review D **30**, 272 (1984).
[6] B. W. Lynn, A. E. Nelson, and N. Tetradis, Nuclear Physics B **345**, 186 (1990).
[7] B. W. Lynn, "Liquid phases in SU(3) Chiral Perturbation Theory: Drops of Strange Chiral Nucleon Liquid and Ordinary Chiral Heavy Nuclear Liquid," (2010), arXiv:1005.2124.
[8] A. R. Zhitnitsky, JCAP **0310**, 010 (2003).
[9] E. Pontón, Y. Bai, and B. Jain, Journal of High Energy Physics **2019** (2019), 10.1007/s13130-019-11194-5.
[10] D. M. Jacobs, G. D. Starkman, and B. W. Lynn, Monthly Notices of the Royal Astronomical Society **450**,

3418 (2015).
[11] D. M. Jacobs, A. Weltman, and G. D. Starkman, Physical Review D **91**, 115023 (2015).
[12] J. S. Sidhu, R. J. Scherrer, and G. Starkman, "Death by dark matter," (2019), arXiv:1907.06674.
[13] J. S. Sidhu and G. Starkman, "Macroscopic dark matter constraints from bolide camera networks," (2019), arXiv:1908.00557.
[14] J. S. Sidhu, R. M. Abraham, C. Covault, and G. Starkman, JCAP **1902**, 037 (2019), arXiv:1808.06978 [astro-ph.HE].
[15] J. S. Sidhu, G. Starkman, and R. Harvey, Physical Review D **100** (2019).
[16] A. De Rujula and S. L. Glashow, Nature **312**, 734 (1984).
[17] P. B. Price, Physical Review D **38**, 3813 (1988).
[18] P. W. Graham, R. Janish, V. Narayan, S. Rajendran, and P. Riggins, Physical Review D **98**, 115027 (2018).
[19] M. A. et al. and, The European Physical Journal C **25**, 511 (2002).
[20] C. Alcock *et al.*, The Astrophysical Journal **550**, L169 (2001).
[21] P. Tisserand *et al.*, Astronomy & Astrophysics **469**, 387 (2007).
[22] B. J. Carr, K. Kohri, Y. Sendouda, and J. Yokoyama, Physical Review D **81**, 104019 (2010).
[23] K. Griest, A. M. Cieplak, and M. J. Lehner, Physical Review Letters **111**, 181302 (2013).
[24] H. Niikura *et al.*, Nature Astronomy **3**, 524 (2019).
[25] N. Smyth, S. Profumo, S. English, T. Jeltema, K. McKinnon, and P. Guhathakurta, "Updated constraints on asteroid-mass primordial black holes as dark matter," (2019), arXiv:1910.01285.
[26] R. J. Wilkinson, J. Lesgourgues, and C. Boehm, JCAP **4**, 026 (2013), arXiv:1309.7588.
[27] C. Bœhm, P. Fayet, and R. Schaeffer, Physics Letters B **518**, 8 (2001).
[28] J. S. Sidhu and G. D. Starkman, "Reconsidering astrophysical constraints on macroscopic dark matter," (2019), arXiv:1912.04053.
[29] This is the distribution of macro velocities in a non-orbiting frame moving with the Galaxy. When considering the velocity of macros impacting the atmosphere, (1) is modified by the motion of the Sun and Earth in that frame, and by the Sun's and Earth's gravitational potential. We have taken into account these effects (as explained, for example, in [52]), except the negligible effect of Earth's gravitational potential.
[30] S. Davidson, S. Hannestad, and G. Raffelt, Journal of High Energy Physics **2000**, 003 (2000).
[31] S. Dimopoulos, D. Eichler, R. Esmailzadeh, and G. D. Starkman, Physical Review D **41**, 2388 (1990).
[32] A. A. Prinz *et al.*, Physical Review Letters **81**, 1175 (1998).
[33] J. H. Chang, R. Essig, and S. D. McDermott, Journal of High Energy Physics **2018** (2018), 10.1007/jhep09(2018)051.
[34] B. V. Lehmann, C. Johnson, S. Profumo, and T. Schwemberger, Journal of Cosmology and Astroparticle Physics **2019**, 046 (2019).
[35] Y. Bai and J. Berger, "Nucleus capture by macroscopic dark matter," (2019), arXiv:1912.02813.
[36] S. W. Randall, M. Markevitch, D. Clowe, A. H. Gonzalez, and M. Bradač, The Astrophysical Journal **679**, 1173 (2008).
[37] S. Chandrasekhar, The Astrophysical Journal **97**, 255 (1943).
[38] J. Binney and S. Tremaine, *Galactic Dynamics: Second Edition, by James Binney and Scott Tremaine. ISBN 978-0-691-13026-2 (HB). Published by Princeton University Press, Princeton, NJ USA, 2008.* (Princeton University Press, 2008).
[39] A. D. Dolgov, S. L. Dubovsky, G. I. Rubtsov, and I. I. Tkachev, Phys. Rev. D **88**, 117701 (2013).
[40] K. Kadota, T. Sekiguchia, and H. Tashirob, *A new constraint on millicharged dark matter from galaxy clusters*, Tech. Rep. CTPU-16-04 (2016).
[41] Z. J. et al, *SRIM - The Stopping and Range of Ions in Matter* (2008).
[42] D. N. Spergel and P. J. Steinhardt, Phys. Rev. Lett. **84**, 3760 (2000).
[43] M. Rocha, A. H. G. Peter, J. S. Bullock, M. Kaplinghat, S. Garrison-Kimmel, J. Oñorbe, and L. A. Moustakas, Monthly Notices of the Royal Astronomical Society **430**, 81 (2013).
[44] P. S. Epstein, Phys. Rev. **23**, 710 (1924).
[45] M. Benito, A. Cuoco, and F. Iocco, Journal of Cosmology and Astroparticle Physics **2019**, 033 (2019).
[46] C. A. P. Bengaly, C. Clarkson, and R. Maartens, "The hubble constant tension with next generation galaxy surveys," (2019), arXiv:1908.04619.
[47] R. Hellborg, *Electrostatic accelerators: fundamentals and applications* (Springer, 2011).
[48] *Application of Particle and Laser Beams in Materials Technology (Nato Science Series E:)* (Springer, 2010).
[49] P. W. Graham, S. Rajendran, and J. Varela, Physical Review D **92**, 063007 (2015).
[50] F. X. Timmes and S. E. Woosley, The Astrophysical Journal **396**, 649 (1992).
[51] *Spacetime and Geometry: An Introduction to General Relativity* (Pearson International, 1970).
[52] K. Freese, M. Lisanti, and C. Savage, Reviews of Modern Physics **85**, 1561 (2013).